Griffiths, D. V. & Fenton, G. A. (1993). *Géotechnique* 43, No. 4, 577–587

Seepage beneath water retaining structures founded on spatially random soil

D. V. GRIFFITHS* and GORDON A. FENTON†

The effect of stochastic soil permeability on confined seepage beneath water retaining structures has been studied. Random field concepts for the generation of soil permeability properties with a fixed mean, standard deviation and spatial correlation structure have been combined with finite element methods to perform Monte Carlo simulations of the seepage problem. Analyses have been performed for a dam with two cut-off walls. The results of parametric studies to gauge the effect of the standard deviation and correlation structure of the permeability on the output statistics relating to seepage quantities, exit gradients and uplift pressures are presented. In all cases, comparison is made with results that would be achieved on a deterministic basis. Flow rates and other quantities are shown to be affected significantly by the standard deviation and the correlation structure of soil permeability.

KEYWORDS: cut-off walls and barriers; dams; numerical modelling and analysis; permeability; seepage; statistical analysis.

L'article étudie l'influence de la perméabilité d'un sol stochastique sur l'infiltration confinée existant sous une structure de retenue d'eau. Des analyses aléatoires, permettant de générer les propriétés de perméabilité du sol pour une moyenne, un écart-type et un facteur de corrélation donnés, ont été combinées à des méthodes par éléments finis afin de réaliser des simulations de Monte-Carlo pour l'infiltration. Des analyses ont été réalisées pour un barrage comportant deux parois étanches. L'on présente les résultats de l'étude paramétrique réalisée afin de quantifier l'influence de l'écart-type et du facteur de corrélation de la perméabilité sur les statistiques relatives aux quantités infiltrées, au gradient de sortie et aux pressions ascendantes. Dans chacun des cas, des comparaisons ont été établies avec les résultats que l'on aurait obtenus à partir d'une base déterministe. Les débits et autres quantités semblent être significativement affectés par l'écart-type et le facteur de corrélation de la perméabilité du sol.

INTRODUCTION

Most geotechnical analysis is deterministic in that the soil properties used are assumed to be average values. Variations in the soil properties are then accounted for by the use of safety factors which are often applied arbitrarily to the computed result.

This average approach to the definition of soil properties has tended to be applied not only to classical soil mechanics calculations, but also to numerical computations using sophisticated numerical techniques such as the finite element (FE) method. Properties are usually assigned on the basis of a limited number of laboratory tests. In reality, these properties vary from point to point and can be determined deterministically only through numerous field tests. Since this is expensive and impractical, random field models can be used to represent the geomaterial. The parameters of these models can be estimated from a limited number of test results.

Mean soil properties are fairly well established, and recently there has been an improvement in the availability of data on second moment statistics (standard deviation and spatial correlation). The data gathering has been motivated largely by the availability of random field simulation algorithms and their potential for producing useful results. The increased performance of computers has also enabled more detailed discretization of boundary value problems, and better modelling of the statistical properties of the input parameters.

The FE method is an ideal vehicle for modelling materials with a spatial variation in properties. Stochastic FE analysis has been implemented in a number of areas of geotechnical interest (see, e.g., Beacher & Ingra (1981) and Righetti & Harrop-Williams (1988) for stress analysis and settlements of foundations, Ishii & Suzuki (1987) for slope stability and Smith & Freeze (1979a, 1979b) for confined seepage).

Discussion on this Paper closes 5 April 1994; for further details see p. ii.

* University of Manchester.
† Technical University of Nova Scotia.

Stochastic FE can be interpreted in different ways. Statistical properties can be built into the FE equations themselves (see for example Vanmarcke and Grigoriu (1983)), or multiple analyses (Monte Carlo) can be performed, with each analysis stemming from a realization of the soil properties treated as a multi-dimensional random field. In the present work the latter approach has been used to examine confined seepage, with particular reference to flow under a water retaining structure founded on stochastic soil. While the Monte Carlo approach tends to be computationally intensive, it has the advantage of being able to model highly variable input properties.

CONFINED SEEPAGE

In the study of seepage through soils beneath water retaining structures, three important quantities need to be assessed by the designers (Fig. 1): seepage quantity, exit gradients and uplift forces. The classical approach used by civil engineers to estimate these quantities involves the use of carefully drawn flow nets (Casagrande, 1940; Cedergren, 1967; Verruijt, 1970). However, various alternatives to flow nets are available for solution of the seepage problem: in order to perform quick parametric studies, for example relating to the effect of cut-off wall length, powerful approximate techniques such as the method of fragments (Pavlovsky, 1933; Harr, 1962; Griffiths, 1984) are increasingly employed. The conventional methods are deterministic in that the soil permeability is assumed to be constant and homogeneous, although anisotropic properties and stratification can be taken into account.

In this Paper, an approach to the modelling of soil properties is adopted whereby the permeability of the soil underlying a structure such as that shown in Fig. 1 is assumed to be stochastic, i.e. the soil property in question is assumed to be a 'random' field (see, e.g., Vanmarcke, 1984) with certain statistics. Although the best-known statistics are the mean and standard deviation, it is well known that spatial dependencies also exist—the soil properties at two points separated by 1 cm are likely to be more similar than those at two points separated by 1 m or 1 km. This spatial dependence is often characterized by the scale of fluctuation which, loosely, is the distance over which properties show appreciable correlation. In general, for a site of fixed size, as the scale of fluctuation increases the soil properties become more uniform over the site.

The analysis in this Paper uses a technique called local average subdivision (LAS) to generate realizations of the random permeability fields with given mean, standard deviation and correlation structure. This technique is fully described by Fenton (1990) and Fenton & Vanmarcke (1990). The resulting field of permeabilities is mapped on to an FE mesh, and potential and stream function boundary conditions are specified. The governing elliptic equation for steady flow (Laplace) leads to a system of linear equilibrium equations which are solved for the nodal potential values throughout the mesh by use of conventional Gaussian elimination.

Only deterministic boundary conditions are considered in this Paper, the primary goal being to investigate the effects of randomly varying soil properties on the engineering quantities already noted. The method is easily extended to random boundary conditions corresponding to uncertainties in upstream and downstream water levels.

A brief description of the FE technique and the method by which permeability values are assigned to the mesh is given. The statistics of the output quantities relating to flow rate, exit gradients and uplift are discussed.

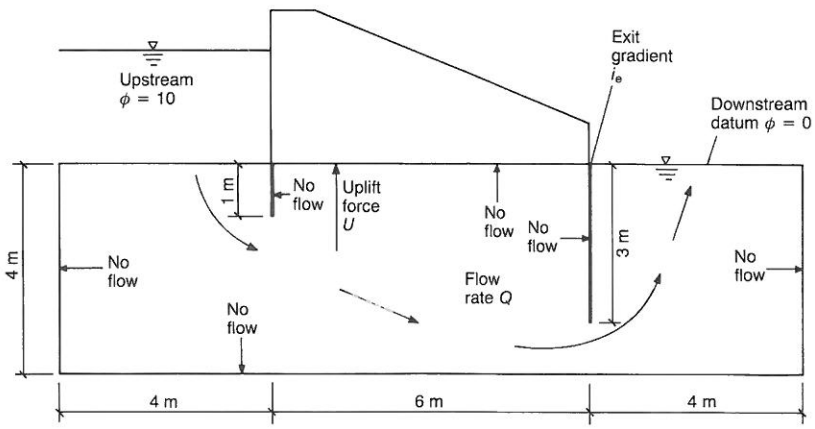

Fig. 1. The boundary value problem

FINITE ELEMENT ANALYSES

The steady flow problem is governed in two dimensions by Laplace's equation, in which the dependent variable ϕ is the piezometric head or potential at any point in the Cartesian field x–y

$$k_x \frac{\partial^2 \phi}{\partial x^2} + k_y \frac{\partial^2 \phi}{\partial y^2} = 0 \tag{1}$$

where k_x and k_y are the permeabilities in the x and y directions. In the present work and at the element level, the permeability field is assumed to be isotropic ($k_x = k_y = k$). While the method discussed here is easily extended to the anisotropic case (through the generation of a pair of correlated random fields), it is felt that such an extension is best restricted to a particular site of interest, the complexity it introduces to a general discussion being unwarranted.

Equation (1) is strictly valid only for constant k. In this analysis the permeability is taken to be constant within each element, its value being given by the local geometric average of the permeability field within the domain of the element. From element to element, the value of k will vary, however, reflecting the random nature of the permeability. This approximation of the permeability field is consistent with the approximations in the FE method and is superior to most traditional approaches, in which the permeability of an element is taken to be simply the permeability at some point within the element.

A typical FE mesh used in this study is shown in Fig. 2. It contains 1400 elements, and represents a model of two-dimensional flow beneath a dam that includes two cut-off walls. The upstream and downstream potential values are fixed at 10 m and 0 m respectively. The cut-off walls are assumed to have zero thickness; the nodes along these walls have two potential values corresponding to the right and left sides of the wall.

The FE code for the solution of Laplace's equation is broadly similar to that given by Smith & Griffiths (1988). The element conductivity matrices are assembled into a global matrix in the usual way, resulting in a system of linear equations in the 'unknown' nodal potential values. The global conductivity relationship after assembly becomes

$$\mathbf{K}\boldsymbol{\Phi} = \boldsymbol{Q} \tag{2}$$

Once the global conductivity equations are solved leading to nodal potential values held in $\boldsymbol{\Phi}$, the output quantities relating to flow rates, uplift pressures and exist gradients are easily deduced. More details on how these values are obtained are given later.

For each boundary value problem considered, multiple solutions were obtained by use of successive realizations of the permeability field. The random permeability field is characterized by three parameters defining its first two moments, namely the mean μ_k, the standard deviation σ_k and the scale of fluctuation θ_k. In order to obtain reasonably accurate estimates of the output statistics, it was decided that each run would comprise the analysis of 1000 realizations. Using the mesh of Fig. 2, the Manchester University Amdahl vector processor (VP1100) typically took about 8 min of CPU time to generate the random field realizations and perform the FE analysis 1000 times.

GENERATION OF PERMEABILITY VALUES

Field measurements of permeability have indicated an approximately log–normal distribution (see, e.g., Hoeksema & Kitanidis, 1985; Sudicky, 1986). The same distribution has therefore been adopted for the simulations generated in this Paper. Essentially, the permeability field is obtained through the transformation

$$k_i = \exp\left(\mu_{\ln k} + \sigma_{\ln k} g_i\right) \tag{3}$$

where k_i is the permeability assigned to the ith element, g_i is the local average of a standard Gaussian random field g over the domain of the ith element, and $\mu_{\ln k}$ and $\sigma_{\ln k}$ are the mean and standard deviation of the logarithm of k

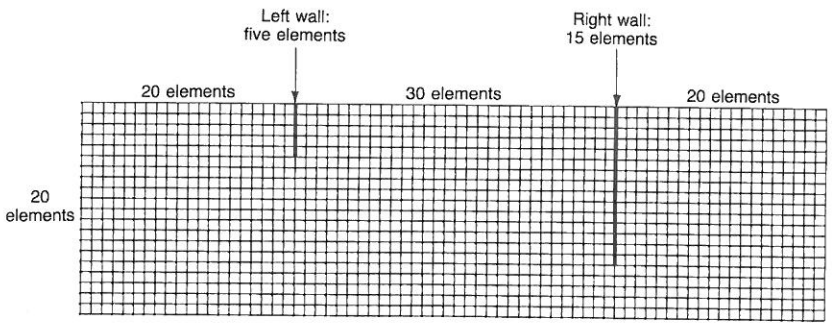

Fig. 2. The FE mesh: all elements are 0·2 m × 0·2 m squares

(obtained from the target mean and standard deviation μ_k and σ_k).

The LAS technique gives realizations of the local averages g_i that are derived from the random field g having zero mean, unit variance and a spatial correlation controlled by the scale of fluctuation. As the scale of fluctuation goes to infinity, g_i becomes equal to g_j for all elements i and j, i.e. the field of permeabilities tends to become uniform on each realization. At the other extreme, as the scale of fluctuation goes to zero, g_i and g_j become independent for all $i \neq j$—the soil permeability changes rapidly from point to point.

In the two-dimensional analyses presented in this Paper, the scales of fluctuation in the vertical and horizontal directions are taken to be equal (isotropic) for simplicity. For a layered soil mass the horizontal scale of fluctuation is generally larger than the vertical scale due to the natural stratification of many soil deposits. The two-dimensional model used here implies that the out-of-plane scale of fluctuation is infinite—soil properties are constant in this direction—which is equivalent to specifying that the streamlines remain in the plane of the analysis. Although this is a deficiency of the present model, it is believed that useful information on the variability of flow quantities can be gained. Further details of the simulation approach for random fields of the type used in this Paper are given by Fenton (1990) and Fenton & Vanmarcke (1990).

DETERMINISTIC SOLUTION

For the seepage problem shown in Fig. 2, a deterministic analysis was performed in which the permeability of all elements was assumed to be 10^{-5} m/s and constant. This value of permeability is typical for very fine sands and silts, and was also used as the mean of subsequent stochastic analyses. Both the potential and inverse streamline problems were solved, leading to the flow net shown in Fig. 3.

All output quantities were computed in non-dimensional form. In the case of the flow rate, the global flow vector $\boldsymbol{Q}$ was computed by forming the product of the potentials and the global conductivity matrix from equation (2). Assuming no sources or sinks in the flow regime, the only non-zero values in $\boldsymbol{Q}$ correspond to the freedoms on the upstream side at which the potentials were fixed equal to 10 m. These values were summed to give the flow rate Q in m^3/s per m, leading to a non-dimensional flow rate $\bar{Q}$ defined by

$$\bar{Q} = Q/(\mu_k H) \tag{4}$$

where μ_k is the (isotropic) mean permeability and H is the total head difference between the upstream and downstream sides. $\bar{Q}$ is equivalent to the number of flow channels divided by the number of equipotential drops n_f/n_d that would be observed in a carefully drawn flow net; it is also equal to the reciprocal of the form factor used in the method of fragments.

The uplift force on the base of the dam U was computed by integration of the pressure distribution along the base of the dam between the cut-off walls. This quantity was easily deduced from the potential values at the nodes along this line together with a simple numerical integration scheme (repeated trapezium rule). A non-dimensional uplift force $\bar{U}$ was defined

$$\bar{U} = U/(H\gamma_w L) \tag{5}$$

where γ_w is the unit weight of water and L is the distance between the cut-off walls. $\bar{U}$ is the uplift force expressed as a proportion of the buoyancy force that would occur if the dam were submerged in water alone.

The exit gradient i_e is the rate of change of head at the exit point closest to the dam at the downstream end. This was calculated using a four-point backward difference numerical differentiation formula of the form

$$i_e \approx (11\phi_0 - 18\phi_{-1} + 9\phi_{-2} - 2\phi_{-3})/6b \tag{6}$$

where the ϕ_i values correspond to the piezometric head at the four nodes vertically below the exit point as shown in Fig. 4, and b is the constant vertical distance between nodes. The downstream potential head is fixed equal to zero, thus $\phi_0 =$ 0·0 m. The use of this four-point formula was

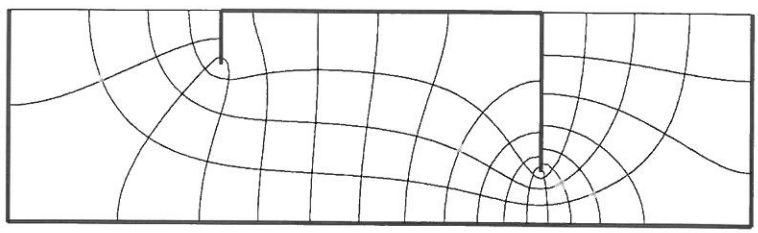

Fig. 3. Deterministic flow net: $n_f = 4$, $n_d = 18$

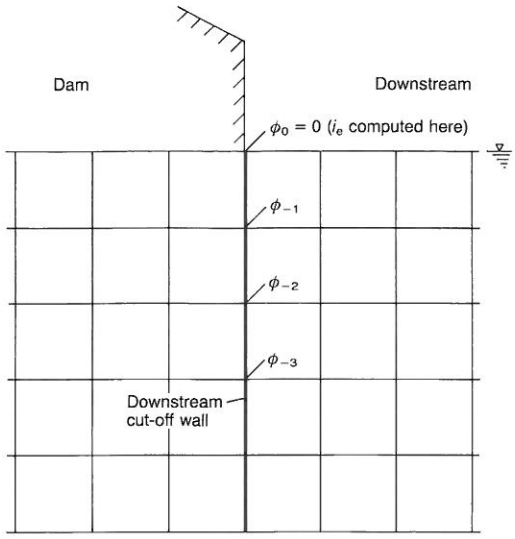

Fig. 4. Detail of downstream cut-off wall

arbitrary, and was regarded as a compromise between the use of very low-order formulae which would be too sensitive to 'random' fluctuations in the potential, and high-order formulae which would involve the use of correspondingly high order interpolation polynomials that would be difficult to justify physically.

With reference to Figs 1 and 2, the constants described were given the values

$$H = 10 \text{ m}$$
$$\mu_k = 10^{-5} \text{ m/s}$$
$$\gamma_w = 9{\cdot}81 \text{ kN/m}^3$$
$$L = 6 \text{ m}$$
$$b = 0{\cdot}2 \text{ m}$$

A deterministic analysis using the mesh of Fig. 2 led to the output quantities

$$\bar{Q} = 0{\cdot}226$$
$$\bar{U} = 0{\cdot}671$$
$$i_e = 0{\cdot}688$$

This value of i_e would be considered unacceptably high for design purposes, as the critical hydraulic gradient for most soils is approximately unity, and a factor of safety against piping of 4–5 is often recommended (see, e.g., Harr, 1962). However, this value of i_e is proportional to the head difference H, which in this study has been set to 10 m for the sake of simplicity and convenience of normalization.

STOCHASTIC ANALYSES

In all the two-dimensional stochastic analyses that follow, the soil was assumed to be isotropic with a mean permeability of $\mu_k = 10^{-5}$ m/s. More specifically, the random fields were generated such that the target (geometric) mean permeability of each FE was held constant at 10^{-5} m/s. Parametric studies were performed on the effect of variation of the standard deviation σ_k and the scale of fluctuation θ_k of the permeability field. After 1000 realizations, statistics relating to output quantities $\bar{Q}$, $\bar{U}$ and i_e were calculated.

Single realization

An example of what a flow net might look like for a single realization is shown in Fig. 5 for permeability statistics $\mu_k = 10^{-5}$ m/s, $\sigma_k = 10^{-5}$ m/s and $\theta_k = 1{\cdot}0$ m. In Fig. 5(a), the flow net is superimposed on a grey scale which indicates the spatial distribution of the permeability values. The correlation length of 1 m can easily be observed.

Dark areas correspond to low permeability and light areas to high permeability. The streamlines clearly try to avoid the low permeability zones, but this is not always possible, as some realizations may generate a complete blockage of low permeability material in certain parts of the flow regime. This type of blockage is most likely to occur where the flow route is compressed, e.g. under a cut-off wall. Flow in these (dark) low permeability zones is characterized by the streamlines moving further apart and the equipotential moving closer together. Conversely, flow in the (light) high permeability zones is characterized by the equipotentials moving further apart and the streamlines moving closer together.

Figure 5(b) shows exactly the same result as Fig. 5(a), but more streamlines have been included and the equipotentials have been removed in order to highlight the contrast between stochastic flow and flow through a deterministic field such as that shown in Fig. 3. Although local variations in the permeability have an obvious effect on the local paths taken by the water as it flows downstream, globally the stochastic and deterministic flow nets show many similarities. The flow is predominantly in a downstream direction, with the fluid flowing down, under and around the cut-off walls. For this reason the statistics of the output quantities might be expected to be insensitive to the geometry of the problem (e.g. the length of walls), and qualitatively similar to the properties of a one-dimensional flow problem.

Statistics of the potential field

Figures 6 and 7 give contours of the mean and standard deviation of the potential field following 1000 realizations for two cases: $\theta_k = 1{\cdot}0$ m and 8·0 m respectively. These values were chosen

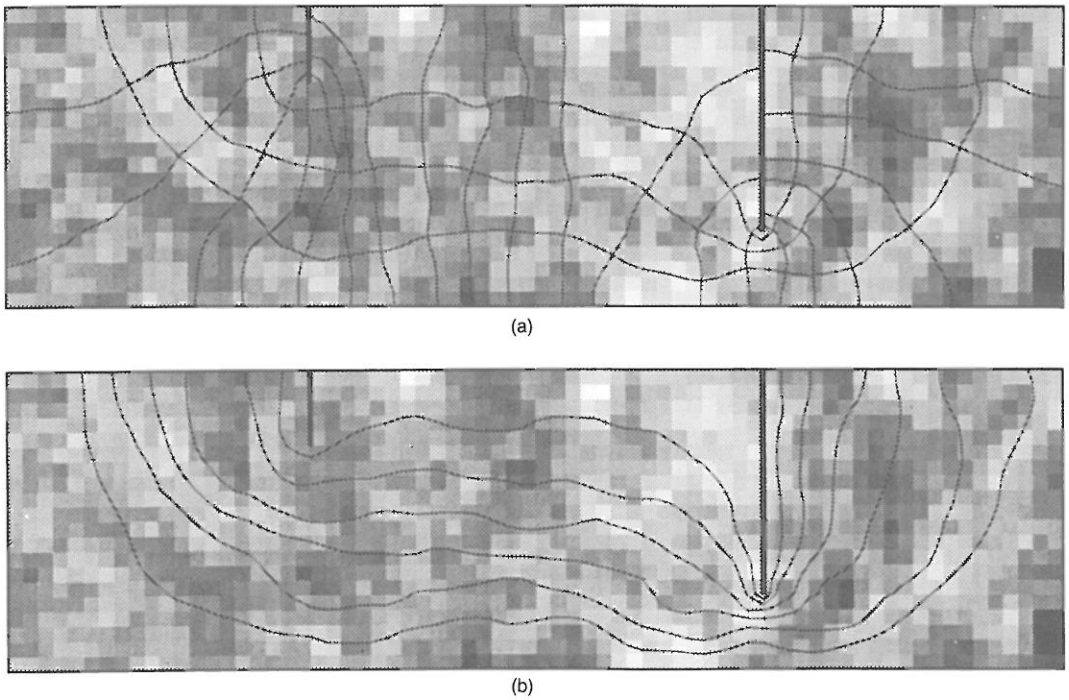

Fig. 5. (a) Stochastic flow net for a single realization ($\mu_k = 10^{-5}$ m/s, $\sigma_k = 10^{-5}$ m/s, $\theta_k = 1{\cdot}0$ m, $n_f = 4$, $n_d = 21$); (b) as (a), with more channels

to represent a weakly correlated soil deposit and a strongly correlated soil deposit respectively. In both cases the standard deviation of the permeability field is set equal to $\sigma_k = 16 \times 10^{-5}$ m/s. This high value of standard deviation was chosen to exaggerate the difference between the stochastic approach and a deterministic approach in which σ_k is effectively zero.

The contours of potential shown in Figs 6 and 7 follow the approach used by Smith & Freeze

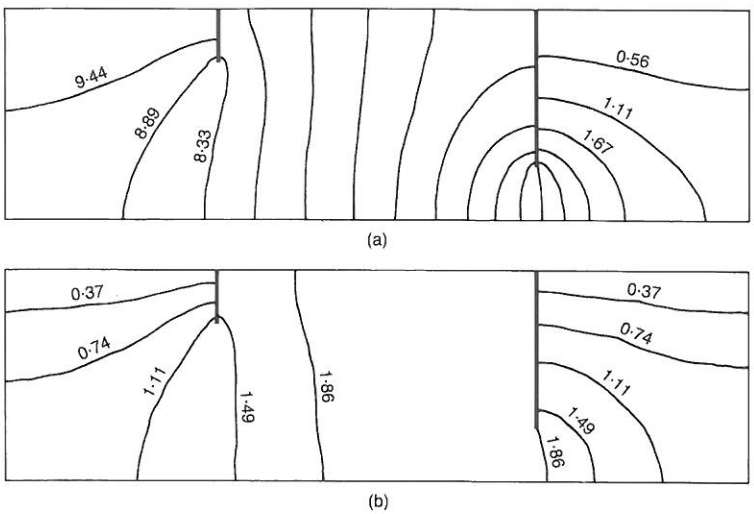

Fig. 6. (a) Contours of mean potential values ($\sigma_k/\mu_k = 16{\cdot}0$, $\theta_k = 1{\cdot}0$ m, contour interval = 0·56 m); (b) contours of potential standard deviation values ($\sigma_k/\mu_k = 16{\cdot}0$, $\theta_k = 1{\cdot}0$ m, contour interval = 0·37 m)

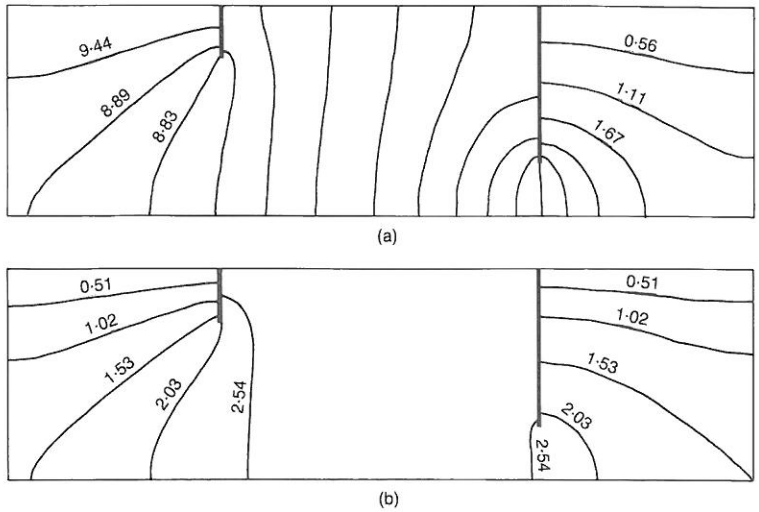

Fig. 7. (a) Contours of mean potential values ($\sigma_k/\mu_k = 16{\cdot}0$, $\theta_k = 8{\cdot}0$ m, contour interval = 0·56 m); (b) contours of potential standard deviation values ($\sigma_k/\mu_k = 16{\cdot}0$, $\theta_k = 8{\cdot}0$ m, contour interval = 0·51 m)

(1979a, 1979b), who presented the results of a series of numerical experiments on both one-dimensional and two-dimensional confined flow problems.

The mean potential values given in Figs 6(a) and 7(a) are very similar to those obtained in the deterministic analysis summarized in the flow net of Fig. 3. The standard deviation of the potentials given in Figs 6(b) and 7(b) indicates the zones of greatest uncertainty regarding the potential values. The upstream and downstream (boundary) potentials are deterministic, so the standard deviation of the potentials on these boundaries equals zero. The greatest values of standard deviation occur in the middle of the flow regime, which in the case considered here represents the zone beneath the dam and between the cut-off walls. The standard deviation is virtually constant in this zone, but is clearly affected by the value of θ_k. The higher the value of θ_k, the greater are the standard deviation values. However, for values of θ_k much larger than the physical size of the flow domain, the variance of the potential field is expected to drop towards zero because the soil permeability becomes uniform throughout the domain.

Parametric studies

The parametric studies based on the mesh of Fig. 2 were designed to show the effect of the permeability's standard deviation σ_k and scale of fluctuation θ_k on the output quantities $\bar{Q}$, $\bar{U}$ and i_e. In all cases the mean permeability μ_k was maintained constant at 10^{-5} m/s.

Instead of plotting σ_k directly, the dimensionless coefficient of variation of permeability was used, and the values $\sigma_k/\mu_k = 0{\cdot}125$, 0·25, 0·50, 1·0, 2·0, 4·0, 8·0 and 16·0 were considered, together with scale of fluctuation values given by $\theta_k = 0{\cdot}0$, 1·0, 2·0, 4·0 and 8·0 m. The case of $\theta_k = 0{\cdot}0$ is obtained simply by taking the cell permeabilities to be mutually independent and governed by the point distribution. It is believed that the ranges given cover most practical situations. All permutations of these values were analysed. The results are summarized in Figs 8–10 in the form of the logarithm (base 10) of σ_k/μ_k plotted against the means and standard deviations of $\bar{Q}$, $\bar{U}$ and i_e, denoted ($\mu_{\bar{Q}}$, $\sigma_{\bar{Q}}$), ($\mu_{\bar{U}}$, $\sigma_{\bar{U}}$) and (μ_{i_e}, σ_{i_e}) respectively.

Flow rate. Figure 8(a) shows a significant fall in $\mu_{\bar{Q}}$ as σ_k/μ_k increases for $\theta_k < 8$ m. As the scale of fluctuation approaches infinity, the expected value of $\bar{Q}$ approaches the constant 0·226. This curve is also shown in Fig. 8(a), having been obtained through theory rather than simulation. In agreement with this result, the curve $\theta_k = 8$ m shows a less marked reduction in $\mu_{\bar{Q}}$ with increasing coefficient of variation σ_k/μ_k. However, over typical scales of fluctuation, the effect on average flow rate is slight. The decrease in flow rate as a function of the variability of the soil mass is important from the point of view of design. Traditional design practice may be relying on this variability to reduce flow rates on average. It also implies that ensuring higher uniformity in the foundation soils may be unwarranted unless the mean permeability is known to be substantially reduced and/or the permeability throughout the

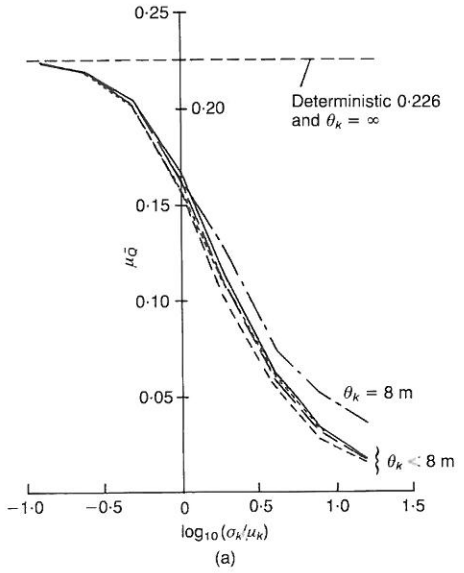

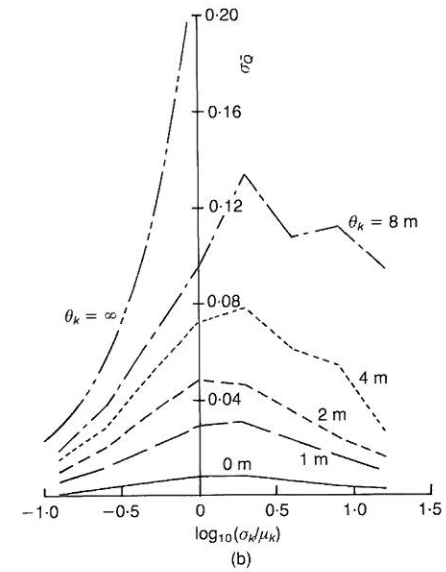

Fig. 8. Coefficient of variation of permeability plotted against: (a) mean flow rate; (b) standard deviation of flow rate

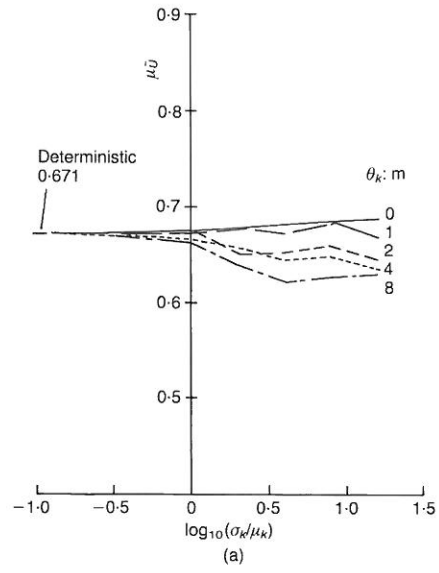

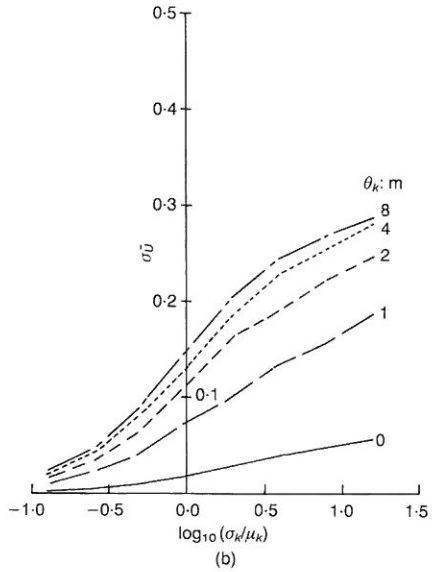

Fig. 9. Coefficient of variation of permeability plotted against: (a) mean uplift force; (b) standard deviation of uplift force

site is carefully measured. The deterministic result $\bar{Q} = 0{\cdot}226$ is included in Fig. 8(a): as expected, the stochastic results converge on this value as σ_k/μ_k approaches 0.

Figure 8(b) shows the behaviour of $\sigma_{\bar{Q}}$ as a function of σ_k/μ_k. Note that $\sigma_{\bar{Q}}$ reaches a maximum corresponding to σ_k/μ_k in the range 1·0–2·0 for $\theta_k < 8$ m. Again, the theoretical result corresponding to $\theta_k = \infty$ has been plotted on the figure, showing a continuous increase with σ_k/μ_k. The reason for the maximum in the simulation results is not clear, but the trend showing a general increase in $\sigma_{\bar{Q}}$ with increasing θ_k is expected. In general, it appears that the greatest variability in $\bar{Q}$ occurs under typical conditions: scales of fluctuation of 1–4 m and coefficient of variation of permeability of about 1 or 2 (see, e.g., de Marsily 1985).

Uplift force. Figure 9 shows the relationship between uplift force parameters $\mu_{\bar{U}}$ and $\sigma_{\bar{U}}$ and

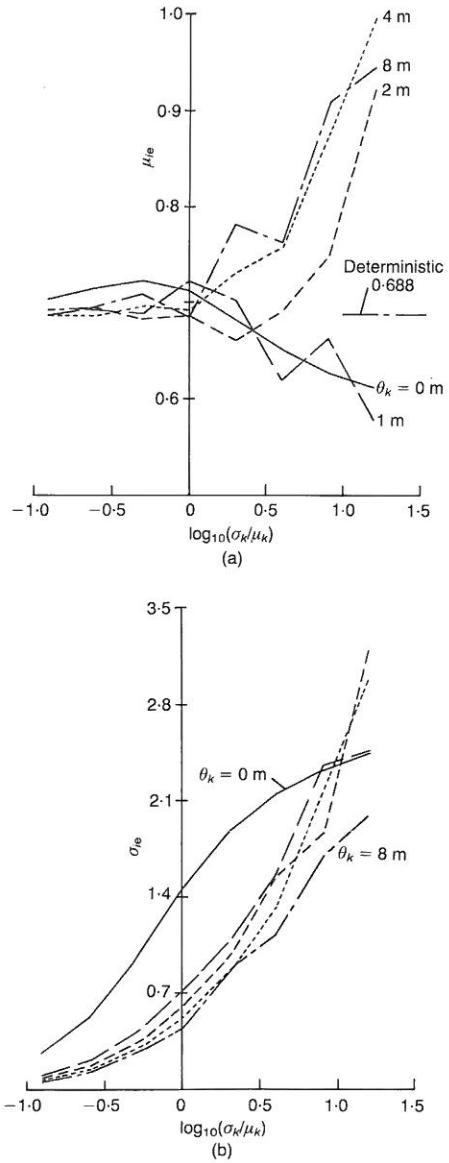

Fig. 10. Coefficient of variation of permeability plotted against: (a) mean exit hydraulic gradient; (b) standard deviation of exit hydraulic gradient

input permeability parameters σ_k/μ_k and θ_k. From Fig. 9(a), $\mu_{\bar{v}}$ is relatively insensitive to the parametric changes. There is a gradual fall in $\mu_{\bar{v}}$ as both σ_k/μ_k and θ_k increase, the greatest reduction being 10% of the deterministic value 0·671 when $\sigma_k/\mu_k = 16{\cdot}0$ and $\theta_k = 8{\cdot}0$ m. The insensitivity of the uplift force to the permeability input statistics might have been predicted from Fig. 3, 6(a) and 7(a), in which the contours of (mean) piezometric head are virtually the same in the deterministic and stochastic analyses.

Figure 9(b) shows that $\sigma_{\bar{v}}$ rises consistently as both σ_k/μ_k and θ_k increase. It is known that in the limit as $\theta_k \to \infty$, $\sigma_{\bar{v}} \to 0$, since under those conditions the permeability field becomes completely uniform. Some hint of this increase followed by a decrease is seen in Fig. 9(b), in that the largest increases are for $\theta_k = 0$–1 m, the increase from $\theta_k = 48$ m being much smaller.

The actual value of $\sigma_{\bar{v}}$ for a given set of σ_k/μ_k and θ_k could easily be deduced from the standard deviation of the potential values. Figs 6(b) and 7(b) give contours of the standard deviation of the potential values throughout the flow domain for the particular values $\sigma_k/\mu_k = 16{\cdot}0$ and $\theta_k = 1{\cdot}0$ and 8·0 m respectively. In Fig. 6(b) the potential standard deviation beneath the dam is approximately constant and equal to 1·86 m; in Fig. 7(b) this value is 2·54 m. After non-dimensionalization by division by $H = 10$ m, these values agree closely with the corresponding values in Fig. 9(b).

The magnitude of the standard deviation of the uplift force given in Fig. 9(b) across the range of parameters considered was not great, implying that this quantity can be estimated with a reasonable degree of confidence. The explanation is that the uplift force is calculated using potential values over a large number of nodes beneath the dam. This 'averaging' process tends to damp out fluctuations in the potential values that would be observed on a local scale, resulting in a variance reduction.

Exit gradient. This quantity is based on the first derivative of piezometric head or potential with respect to distance at the exit point closest to the downstream end of the dam. It is well known that in a deterministic approach, the largest and hence the most critical value of i_e lies at the exit point of the uppermost (and shortest) streamline. While for a single realization of a stochastic analysis this may not be the case, on average the location of the critical exit gradient is expected to occur at the 'deterministic' location.

As i_e is based on a first derivative at a particular location within the mesh (see Fig. 4), it is expected to be the most susceptible to local variations generated by the stochastic approach. In order to average the calculation of i_e over a few nodes, it was decided to use a four-point (backward) finite difference scheme as given in equation (6). This is equivalent to fitting a cubic polynomial over the potential values calculated at the four nodes closest to the exit point adjacent to the downstream cut-off wall. The cubic is then differentiated at the required point to estimate i_e. The gradient is estimated by study of the fluctuations over a length of 0·6 m vertically (the elements are 0·2 m × 0·2 m in size). This length is referred to as the 'differentiation length' below.

The variation of μ_{i_e} and σ_{i_e} over the range of

parameters considered is shown in Fig. 10. The sensitivity of i_e to σ_k/μ_k is clearly demonstrated. In Fig. 10(a), μ_{i_e} agrees quite closely with the deterministic value of 0·688 for values of σ_k/μ_k in the range 0·0–1·0, but larger values start to show significant instability and divergence. For $\theta_k \leq 1$, the tendency is for μ_{i_e} to fall below the deterministic value of i_e as σ_k/μ_k is increased; for larger values of θ_k it tends to increase above the deterministic value. The scales 0 and 1 m are, respectively, less than and of the same magnitude as the differentiation length of 0·6 m used to estimate the exit gradient; the scales 2 m, 4 m and 8 m are substantially greater. If this has some bearing on the divergence phenomena seen in Fig. 10(a), it calls into question the use of a differentiation length to estimate the derivative at a point. Regarding the exit gradient, there may be some conflict between the numerical estimation method and random field theory that needs further investigation.

Figure 10(b) indicates the relatively large values of σ_{i_e}, which grow rapidly as σ_k/μ_k is increased. The influence of θ_k in this case is not as great, the results corresponding to $\theta_k = 1{\cdot}0$, 2·0, 4·0 and 8·0 m being quite closely grouped. Theoretically, as $\theta_k \to \infty$, $\mu_{i_e} \to 0{\cdot}688$ and $\sigma_{i_e} \to 0$. There appears to be some evidence of a reduction in σ_{i_e} as θ_k increases: this agrees with the theoretical result. For scales of fluctuation negligible relative to the differentiation length, i.e. $\theta_k = 0$, the variability in i_e is much higher than that for other scales at all permeability variances but the highest. This is perhaps to be expected, since $\theta_k = 0$ yields large fluctuations in permeability within the differentiation length.

CONCLUSIONS

A range of parametric studies have been performed relating to flow beneath a water retaining structure with two cut-off walls founded on a stochastic soil. Random field concepts were used to generate permeability fields with predefined mean, standard deviation and correlation structure. Mean values of permeability are well documented, but there is less information on second-order statistics such as the standard deviation and scale of fluctuation. The parametric studies presented are believed to span all likely soil distributions that might be encountered.

These values were mapped on to an FE mesh consisting of 1400 elements, and for each set of parameters 1000 realizations of the boundary value problem were analysed. In all cases the target mean permeability of each FE was held constant and parametric studies were performed over a range of values of coefficient of variation and scale of fluctuation. The output quantities under scrutiny were the flow rate, the uplift force and the exit gradient, the first two of these being non-dimensionalized for convenience of presentation.

The mean flow rate was found to be relatively insensitive to typical scales of fluctuation, but fell consistently as the variance of the permeability was increased. This may be of some importance in the design of such water retaining structures. The standard deviation of the flow rate consistently increased with the scale of fluctuation, but rose and then fell again as the coefficient of variation was increased. These maxima are currently the subject of further investigations by the Authors.

The mean uplift force was rather insensitive to the parametric variations, falling by only $\sim 10\%$ in the worst case (high permeability variance and $\theta_k = 8$ m). The relatively small variability of uplift force was due to a 'damping out' of local variations inherent in the random field by the averaging of potential values over the nodes along the full length of the base of the dam. Nevertheless, the standard deviation of the uplift force rose consistently with increasing scale of fluctuation and coefficient of variation, as was expected from the contour plots of the standard deviation of the potential values across the flow domain.

The mean exit gradient was much more sensitive to the statistics of the input field. Being based on a first derivative of piezometric head with respect to length at the exit point, this quantity is highly sensitive to local variations inherent in the potential values generated by the random permeability field. Some local averaging was introduced by the use of a four-point numerical differentiation formula; however, the fluctuation in mean values was still considerable and the standard deviation values were high.

ACKNOWLEDGEMENTS

The work described in this Paper was supported in part by a travel grant (ref. 07-04-03-2) from the Association of Universities and Colleges of Canada, a NATO Collaborative Research Grant (CRG 911007) and an SERC Research Grant (GR/H 44066).

NOTATION

- b vertical spacing between nodes
- g standard Gaussian random field
- g_i local average of g over the ith element
- H head difference between upstream and downstream levels
- i_e exit hydraulic gradient
- $\mathbf{K}$ global conductivity matrix
- k permeability
- k_i permeability assigned to the ith element
- k_x, k_y permeability in the x and y directions

L width of dam
n_d number of equipotential drops
n_f number of flow channels
$\underline{Q}$ global flow vector
$Q, \bar{Q}$ flow rate and non-dimensional flow rate
$U, \bar{U}$ uplift force and non-dimensional uplift force
x, y Cartesian co-ordinates
γ_w unit weight of water
θ_k scale of fluctuation of permeability
μ_k, σ_k mean and standard deviation of permeability
$\mu_{\ln k}, \sigma_{\ln k}$ mean and standard deviation of $\ln k_i$
μ_{i_e}, σ_{i_e} mean and standard deviation of exit gradient
$\mu_{\bar{Q}}, \sigma_{\bar{Q}}$ mean and standard deviation of dimensionless flow rate
$\mu_{\bar{U}}, \sigma_{\bar{U}}$ mean and standard deviation of dimensionless uplift force
σ_k/μ_k coefficient of variation of permeability
Φ global potential vector
ϕ potential or piezometric head
$\phi_0, \phi_{-1}, \phi_{-2}, \phi_{-3}$ potential values near exit point

REFERENCES

Beacher, G. B. & Ingra, T. S. (1981). Stochastic FEM in settlement prediction. *J. Geotech Engng Am. Soc. Civ. Engrs* **107**, GT4, 449–463.

Casagrande, A. (1940). *Seepage through dams.* Boston Society of Civil Engineers.

Cedergren, H. R. (1967). *Seepage, drainage and flow nets.* New York: Wiley.

de Marsily, G. (1985). Spatial variability of properties in porous media: a stochastic approach. *Advances in transport phenomena in porous media*, eds J. Bear and M. Y. Corapcioglu, pp. 719–769. Boston: NATO Advanced Study Institute of Fundamentals of Transport Phenomena in Porous Media.

Fenton, G. A. (1990). *Simulation and analysis of random fields.* PhD thesis. Princeton University.

Fenton, G. A. & Vanmarcke, E. H. (1990). Simulation of random fields via local average subdivision. *J. Engng Mech. Am. Soc. Civ. Engrs* **116**, No. 8, 1733–1749.

Griffiths, D. V. (1984). Rationalized charts for the method of fragments applied to confined seepage. *Géotechnique* **34**, No. 2, 229–238.

Harr, M. E. (1962). *Groundwater and seepage.* New York: McGraw-Hill.

Hoeksema, R. J. & Kitanidis, P. K. (1985). Analysis of the spatial structure of properties of selected aquifers. *Wat. Resour. Res.* **21**, No. 4, 563–572.

Ishii, K. & Suzuki, M. (1987). Stochastic finite element method for slope stability analysis. *Struct. Safety* **4**, 111–129.

Pavlovsky, N. N. (1933). Motion of water under dams. *Proc. 1st Congr. Large Dams, Stockholm*, 179–192.

Righetti, G. & Harrop-Williams, K. (1988). Finite element analysis of random soil media. *J. Geotech. Engng Am. Soc. Civ. Engrs* **114**, GT1, 59–75.

Smith, I. M. & Griffiths, D. V. (1988). *Programming the finite element method*, 2nd edn. Wiley.

Smith, L. & Freeze, R. A. (1979a). Stochastic analysis of steady state groundwater flow in a bounded domain. 1. One-dimensional simulations. *Wat. Resour. Res.* **15**, No. 3, 521–528.

Smith, L. & Freeze, R. A. (1979b). Stochastic analysis of steady state groundwater flow in a bounded domain. 2. Two-dimensional simulations. *Wat. Resour. Res.* **15**, No. 6, 1543–1559.

Sudicky, E. A. (1986). A natural gradient experiment on solute transport in a sand aquifer: spatial variability of hydraulic conductivity and its role in the dispersion process. *Wat. Resour. Res.* **22**, No. 13, 2069–2083.

Vanmarcke, E. H. (1984). *Random fields: analysis and synthesis.* Cambridge, Mass.: MIT Press.

Vanmarcke, E. H. & Grigoriu, M. (1983). Stochastic finite element analysis of simple beams. *J. Engng Mech. Am. Soc. Civ. Engrs* **109**, No. 5, 1203–1214.

Verruijt, A. (1970). *Theory of groundwater flow.* London: Macmillan.